Biointerphases

RESEARCH ARTICLE | JUNE 18 2025

Surface potential modulates fibronectin adsorption and molecular interaction on graphene-based materials

Special Collection: Biointerfaces in India

Rohit ; Rachayita Bharadwaj ; Chandrashish Roy; Sourabh Ghosh; Sachin Kumar

Biointerphases 20, 031003 (2025)
https://doi.org/10.1116/6.0004504

Biointerphases
A Journal of Biomaterials and Biological Interfaces

ARTICLE

pubs.aip.org/avs/bip

Surface potential modulates fibronectin adsorption and molecular interaction on graphene-based materials

Cite as: Biointerphases 20, 031003 (2025); doi: 10.1116/6.0004504
Submitted: 18 February 2025 · Accepted: 20 May 2025 ·
Published Online: 18 June 2025

Rohit,[1] Rachayita Bharadwaj,[1] Chandrashish Roy,[2] Sourabh Ghosh,[2] and Sachin Kumar[1,3,a)]

AFFILIATIONS

[1]Centre for Biomedical Engineering, Indian Institute of Technology Delhi, New Delhi 110016, India
[2]Department of Textile and Fibre Engineering, Indian Institute of Technology Delhi, New Delhi 110016, India
[3]Department of Biomedical Engineering, All India Institute of Medical Sciences, New Delhi 110029, India

Note: This paper is part of the Biointerphases Special Topic Collection Biointerfaces in India.
[a)]**Author to whom correspondence should be addressed:** sachin.kumar@cbme.iitd.ac.in

ABSTRACT

Protein interactions on graphene-based materials (GBMs) are predominantly governed by interphase surface properties such as surface chemistry and roughness; however, the critical role of surface potential (SP) in modulating these interactions remains largely unexplored. In this work, we investigated a model study highlighting how two distinct GBMs [graphene oxide (GO) and reduced graphene oxide (RGO)] with different SP regulate protein interactions, spanning from macroscopic adsorption to molecular-level conformational changes. Through thermal reduction, hydrophilic GO was transformed into hydrophobic RGO, generating distinct SP of +120 mV for GO and +60 mV for RGO. This modulation in SP created a platform for differential protein interactions. The influence of SP on protein interactions was evident when fibronectin (FN) was introduced onto GO and RGO surfaces. Quartz crystal microbalance with dissipation and fluorescence microscopy revealed that the distinct SP of GO and RGO surfaces significantly affected FN adsorption. On the RGO substrate, which exhibited a lower SP, FN adsorption was ~3 times greater than on the GO substrate. In contrast, FN on the GO adopted elongated fibrillar structures, driven by strong polar, hydrophilic, and electrostatic interactions at the molecular scale, regulating its conformation upon adsorption. Molecular docking simulations further supported these findings, indicating a stronger and more stable interaction between FN and RGO (binding energy C-score: −3.87, RMSD: 0.01 Å) than between FN and GO (C-score: −2.24, RMSD: 0.42 Å). Overall, this study underscores the pivotal role of SP of GBMs in modulating protein adsorption, binding stability, and conformational organization, providing key insights into the rational design of GBM biomaterials with tailored biointerface properties.

I. INTRODUCTION

Over the years, it is now well demonstrated that adsorbed proteins do not retain their native molecular structure upon interaction with a biomaterial surface; rather, they undergo molecular conformational changes influenced by the surface's physicochemical properties like surface roughness, surface wettability, surface charge, and surface chemistry.[1–3] These changes in protein molecular conformation and orientation on the biomaterial's surface can directly affect cellular processes by altering the availability and activity of functional domains responsible for receptor binding and downstream signalling. Thus, there is a growing need to understand how different biomaterial surface properties influence the molecular structure and functionality of adsorbed proteins. Understanding these interactions at the molecular level is essential for rationally designing biomaterials that can predictably and precisely modulate cell behavior.

In the last few decades, graphene and graphene-based materials (GBMs) like graphene oxide (GO), reduced graphene oxide (RGO), have gained significant attention as promising candidates for the development of biomaterials in tissue engineering applications owing to their unique physiochemical characteristics.[4–7] The unique physicochemical properties (like surface roughness, surface chemistry, and surface potential) of graphene and GBMs have been shown to significantly influence cell response, but how each of these properties influences cell function mediated by its protein-graphene interphase is not

well understood. Few studies have investigated how the surface chemistry of GBMs influences protein interaction at the interphase to influence stem cell response.[8,9] Lee *et al.* showed that insulin adsorbed onto pristine graphene underwent denaturation, whereas insulin retained its bioactive conformation when adsorbed onto GO. As a result, researchers suggested that GO acted as a reservoir of preconcentrated insulin in bioactive form facilitating enhanced interaction with stem cells promoting adipogenic differentiation.[10] On a similar line in our previous study, we highlighted how change in surface chemistry of GO and RGO regulated fibronectin adsorption and its molecular-scale morphology change on GO and RGO surfaces regulating differential Arginine-Glycine-Aspartic acid (Arg-Gly-Asp) domain interaction with stem cells, resulting in differential osteogenic differentiation of stem cells on the GO and RGO surface.[11]

Surprisingly, most studies on protein interactions with GBMs have focused on the effects of surface chemistry, such as functionalization with oxygen-containing groups in GO or chemical reduction in RGO, while largely overlooking the role of surface potential due to inherently interlinked surface chemistry and surface potential in graphene-based materials, making it challenging to isolate their individual effects completely. However, few studies on ceramic biomaterials with calcium phosphate (Ca-P) functional groups, like hydroxyapatite (HA), octacalcium phosphate (OCP), biphasic calcium phosphate (BCP), and β-tricalcium phosphate (β-TCP), which exhibit similar chemical compositions but possess differences in surface charge distribution due to different crystal structure and ion distribution have shown to differently interact with biomolecules and regulate biological responses differently.[12,13] For example, it has been demonstrated that HA with a higher net surface charge and more negative zeta potential exhibits significantly greater adsorption of lysozyme (LSZ) compared to BCP and β-tricalcium phosphate (β-TCP).[14] This is attributed to stronger electrostatic attraction between the positively charged LSZ and the negatively charged HA surface, despite all three materials having comparable surface chemistry. Thus, it is now increasingly evident that surface potential, alongside chemical identity, must be considered a key design parameter in the development of bio-interactive materials.

Similar to ceramic materials, in GBMs, it is well-documented that changes in factors like carbon to oxygen ratio, vacancies, edge irregularities, grain boundaries, and graphene layer thickness (few-layer, typically 2–10 layers) can also contribute to variations in the local electronic environment affecting overall surface potential of GBMs. Panchal et al. showed that increasing the graphene thickness from single-layer graphene (1LG) to bilayer graphene (2LG) results in a measurable shift in surface potential of approximately 25–30 mV.[15] Such variations in layer thickness affecting surface potential have been shown to significantly influence adsorption energetics for small molecules like nitric oxide (NO) and water vapor.[16,17] These results clearly underscore the sensitive nature of GBM surface potential to subtle structural differences, which, in turn, can have significant impact on protein adsorption, orientation, and conformation changes at the material interface. However, the overall effect of surface potential on protein interactions has not been directly evaluated on GBMs due to inherently interlinked surface chemistry and surface potential in graphene-based materials, making it challenging to isolate their individual effects completely. However, in this study, we mainly concentrated on the influence of surface potential of GBM on protein interactions. In this study, we conduct a dedicated model study only highlighting how different surface potentials of GO and RGO can influence fibronectin adsorption at macroscale and its molecular structure and interaction with GO and RGO surfaces.

II. MATERIALS AND METHODS

A. Preparation of GO- and RGO-coated substrates

GO- and RGO-coated substrates were prepared using GO flakes gifted by Parekh Lab, University of Texas, Austin (synthesized by modified hummers methods). Obtained GO flakes were dispersed into ultra-pure water to make 2 mg/ml solution and then batch sonicated for 30 min to obtain homogenously dispersed and exfoliated GO solution. GO solution was spin coated at 2000 rpm for 30 s on clean ultraviolet ozone (UVO) treatment glass surface in accordance with previously reported protocol to obtain a GO-coated substrate.[11,18] Obtained GO-coated substrate was subsequently thermally heated using vacuum oven for 6 h at 200 °C to yield thermally reduced RGO-coated substrate as illustrated in Fig. 1.

B. Characterization of GO- and RGO-coated substrates

The physicochemical properties of obtained GO and thermally reduced RGO-coated substrate were evaluated using various techniques. Surface morphology of GO- and RGO-coated substrates was evaluated using optical and scanning electron microscopy. In brief, the optical image of GO- and RGO-coated glass substrate was acquired using an inverted microscope (LEICA). After taking optical image, GO- and RGO-coated glass substrates were gold sputtered and mounted on a metallic sample holder with a carbon tape, and scanning electron microscope (SEM) imaging was performed using a SEM (LEO Gemini). Atomic force microscopy (AFM, Bruker Dimension Icon) under tapping mode was used to evaluate GO and RGO flakes thickness. Fourier Transform Infrared (FTIR) spectra analysis was performed to investigate the chemical nature of obtained GO- and RGO-coated substrates. FTIR spectra of control clean glass substrate, GO-, and RGO-coated substrates were recorded using ATR-FTIR NICOLET-iS50 spectrometer (ThermoFischer) with ATR mode from 4000 to 400 cm^{-1} range, with a resolution of 4 cm^{-1}. Raman spectra of GO- and RGO-coated substrates were recorded using Raman spectroscopy (uRaman, TechnoSpex) at room temperature with 633 nm laser as an excitation source. X-ray photoelectron spectroscopy (XPS, Omicron) was utilized to assess the difference in chemical composition [Carbon to Oxygen ratio (C:O)] of obtained GO- and RGO-coated substrates using the area under the curve of the oxygen and carbon 1s signals and taking the relative sensitivity factors (RSF) given by photoemission cross sections and analyzer transmission as per reported literature.[19]

C. Surface charge and surface potential measurement of GO- and RGO-coated substrates

Measuring surface charge of the coated film of GO and RGO using zeta potential was challenging; as a result, we carefully scraped off the coated GO and RGO flakes and dispersed them into an appropriate solvent (0.5 mg/ml) to form a stable dispersed

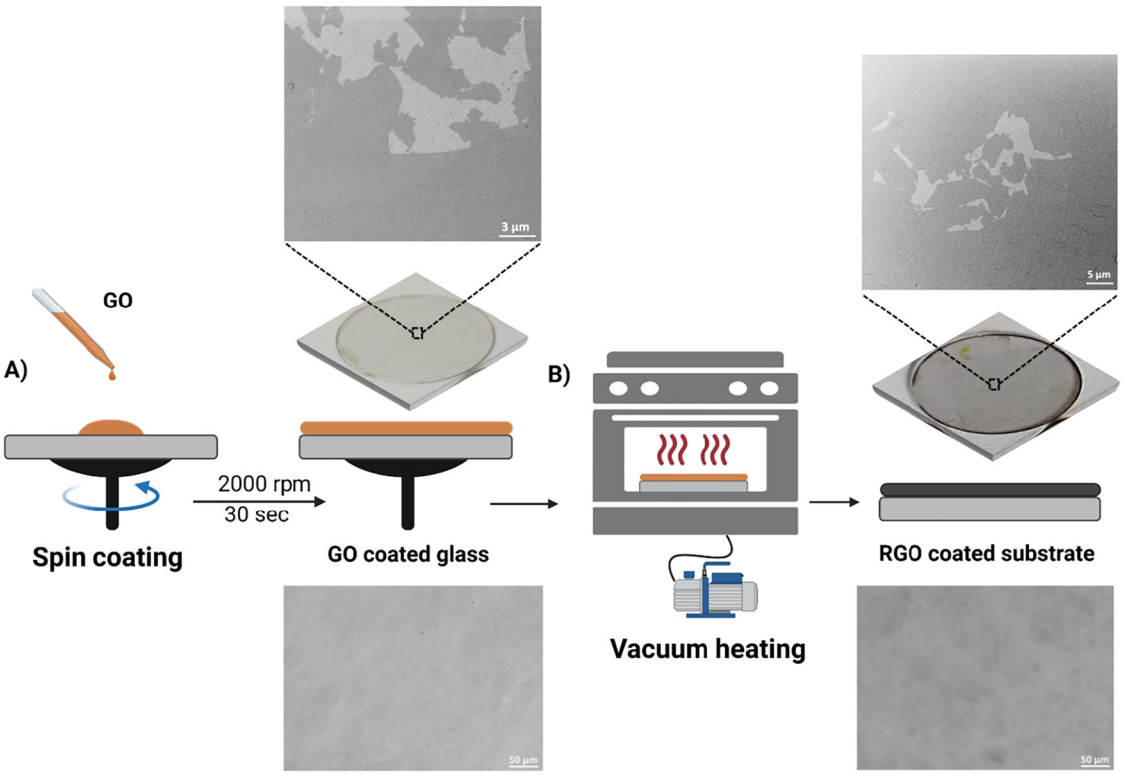

FIG. 1. Schematic representation of the preparation of GO- and RGO-coated glass substrates. (a) Coating of glass with GO using spin coating technique at 2000 rpm for 30 s. (b) Thermal reduction of GO-coated glass using vacuum heating at 200 °C for 6 h to obtain RGO-coated glass substrate.

solution. Later, the surface charge on GO- and RGO-suspended flakes was studied using zeta potential measurements. In brief, 0.5 mg/ml of dispersed GO (in water) and RGO (in chloroform) was prepared using probe sonication for 30 min to form a homogenous dispersed solution and subjected to zeta potential measurements using Zetasizer NanoZS90 (Zetasizer Nano ZS90). Static water contact angle measurements were used to assess the surface wettability of obtained GO- and RGO-coated substrates. The surface potential of the GO- and RGO-coated films was evaluated using Kelvin probe force microscope (KPFM) measurements (KPFM, Bruker Dimension Icon XR) in accordance with reported literature.[20,21] In brief, dispersed GO and RGO solution were drop cast on silica surface, and its surface profile and surface potential were obtained in dual-pass lift mode capturing first the height profile followed by surface potential difference measurement.

D. Protein adsorption study

Spin-coated GO and RGO substrates were placed into 12-well plates, and 10 μg/ml solution of fibronectin (FN) and fluorophore label fibronectin (80:20 ratio) (Sigma-Aldrich) in phosphate-buffered saline (PBS); *p*H 7.4 was added into well plates containing GO and RGO substrates, respectively, and incubated at room temperature for 1 h to allow the FN to adsorb. Protein-adsorbed GO and RGO substrates were gently washed with PBS multiple times to remove non-adsorbed FN. Adsorbed FN on GO and RGO substrates was imaged using a fluorescence microscope (EVOS M7000, ThermoFisher Scientific) under green channel.

Real-time FN adsorption and its molecular interaction on GO and RGO substrates were studied using a quartz crystal microbalance with dissipation monitoring (QCM-D) in accordance with previously established protocol.[11] In brief, the QCM-D sensor (QSensor, QSX 303 SiO_2) was first cleaned and spin coated with GO and RGO sheets as described above. Prepared GO- and RGO-coated QCM-D sensors were equilibrated by using PBS solution at a steady flow rate of 0.1 ml/min for 5 min at room temperature to establish a stable baseline. Thereafter, FN protein solution at a concentration of 10 μg/ml in PBS was introduced, and the adsorption process was monitored in real-time by recording changes in the resonance frequency and dissipation over time, which reflected the mass of FN adsorbed and interaction onto the GO- and RGO-coated sensor surface. The surface mass density of adsorbed FN on GO and RGO substrates was determined using the Sauerbrey equation,

$$\Delta m = -\frac{C}{n}\Delta f,$$

where $C = 17.7$ ng cm^{-2} s^{-1}, n = overtone number, and Δf = frequency

change. For data analysis, overtone number ($n = 3$) was used. Adsorbed FN on GO- and RGO-coated QCM-D sensors was used to evaluate structural features and conformational changes of FN upon adsorption using AFM operated in tapping mode, enabling high-resolution imaging of the FN morphology at nanoscale.

E. Computational modelling study of FN interaction with GO and RGO

Molecular docking simulations were performed to provide a more profound understanding of the molecular interactions that regulate FN adsorption on GBMs. Fibronectin (PDB ID: 1FNF) was retrieved from the RCSB Protein Data Bank,[22] whereas the molecular structures of GO and RGO were constructed using ChemDraw (version 23.1.2). The GO surface comprised approximately 30% oxygenated functional groups, including epoxy, hydroxyl, and carboxyl groups, distributed across the basal plane, whereas the oxygen content in RGO comprised around 10%, indicative of the surface after thermal reduction. The protein structure was pre-processed in UCSF Chimera by eliminating non-essential residues, such as water molecules and heteroatoms, to guarantee precise docking configurations.[23,24] Likewise, GO and RGO structures were examined and refined in UCSF Chimera prior to undergoing docking simulations with AutoDock Vina.[25] A blind docking method was utilized to thoroughly investigate the FN surface and identify potential binding regions on the GBMs. Binding energy (c-score) was employed for analyzing the docking results, and the conformation with the lowest energy was chosen since it revealed the most favorable interaction. To enhance the evaluation of binding quality, hydrophobic interactions between FN and GBMs were analyzed, offering insights into the fundamental mechanisms influencing protein adsorption. Furthermore, root-mean-square deviation (RMSD) values of the docked complexes were computed using PyMOL software to assess the precision and stability of the final protein–ligand interactions. The visualization software (Biovia Discovery Studio Visualizer v24.1.0.23298) was also utilized to analyze the docking results of FN with GO and RGO and to produce interaction illustrations.

F. Statistical analysis

All experimental data, derived from a minimum of three independent experiments, are expressed as mean ± standard deviation. Quantitative data analysis was conducted employing ImageJ (National Institutes of Health, USA), and the results were graphically illustrated using Origin 2024. Statistical comparisons among groups were performed using one-way ANOVA, followed by Tukey's post hoc test for multiple comparisons. Statistical significance was established at $p < 0.05$, denoted by symbols in the corresponding figures.

III. RESULTS AND DISCUSSION

A. Preparation and characterization of GO- and RGO-coated substrates

Graphene oxide (GO), the oxidized form of graphene, is frequently reduced by various methods (like chemical, thermal, hydrothermal, electrochemical, and photocatalytic) to obtain RGO, which exhibits distinct properties compared to its oxidized counterpart for biomedical application. Among these reduction techniques, thermal reduction stands out as a simple, safer, and economic alternative method, allowing precise control over the degree of reduction and enabling the production of two distinct forms of graphene-based materials GO and RGO for biomedical applications. For preparation of GO and RGO substrates, aqueous dispersed GO (2 mg/ml) solution was spin coated on plasma-treated glass cover slip. Spin coating of GO solution leads to rapid removal of the solvent due to spinning that improves the interaction between GO- and plasma-treated hydrophilic glass substrates, which provides strong adhesion with continuous film coating with minimal wrinkling. After coating GO on cleaned plasma-treated glass, a semitransparent brownish color can be seen due to covering of few layers of GO sheets as shown in Fig. 1(a). The GO-coated substrate was later subjected to thermal reduction in accordance to previous report to obtain the RGO-coated substrate.[11] After thermal reduction, the brown color changed to black color, a visible indicator of GO reduction to RGO as shown in Fig. 1(b).

The optical micrographs of the GO-coated substrate showed nearly transparent flaky sheet coverage, whereas the RGO-coated substrate showed visible darkish contrast as shown in Figs. 1(a) and 1(b) (for better contrast, see Fig. S1 in the supplementary material). The darkish contrast and color change from brownish to black for the RGO film can be ascribed to restoration of sp^2 hybridization in graphene sheets enhancing light absorption of RGO sheets in the visible regions. The SEM micrograph of GO- and RGO-coated substrates showed well coverage of GO and RGO sheet like flakes without any wrinkled morphology with a thin coating of 1–3 layers. The wrinkle free and thin coating of GO and RGO can be ascribed to centrifugal force during spinning, which creates a shearing force to align the GO sheets parallel to the substrate surface, minimizing overlapping and ensuring a smooth wrinkle free morphology and uniform thin coverage.

AFM micrograph [Fig. 2(a)] of the GO coating showed thin-coated sheeted flaky morphology with an individual sheet thickness of around 1.2 nm. After thermal treatment, flake thickness decreased to 0.9 nm indicating the removal of oxygenated functional groups from GO surface, in consistent with previous reports.[26] The impact of thermal reduction on chemical functional groups on GO and RGO surfaces was observed in their FTIR spectra [Fig. 2(b)]. It is important to note that the spectral analysis of very thin coatings using FTIR requires careful consideration of the IR transparency of the control substrate to avoid interference and ensures accurate identification of functional groups. To address this, IR spectra of the clean glass substrate were first collected to find IR-sensitive region (Fig. S2 in the supplementary material). The FTIR spectra of the clean glass substrate showed no IR peaks at higher wavenumber from 4000 to 1500 cm^{-1}, whereas at lower wavenumber at around 1400 and 940 cm^{-1}, the control glass substrate showed IR peaks (Fig. S2 in the supplementary material) corresponding to the intrinsic Si–O–Si bending and stretching vibrations typical of silicate-based glass.[27] This observation indicated that IR spectra collected between 4000 and 1500 cm^{-1} on the glass substrate could be appropriate for detecting thin-coated materials as supported by previous studies for analyzing thin immobilized, self-assemble molecules (SAM) or graphene oxide (GO) and its derivatives coating on the glass substrate.[28–30] IR spectra collected from 4000 to 1500 cm^{-1} for the GO-coated glass substrate showed hydroxyl stretching (–OH), CH stretching shoulder, carbonyl (–C = O), and alkenes (–C = C–) functional group peaks at 3000–3500, 2800, 1720, and

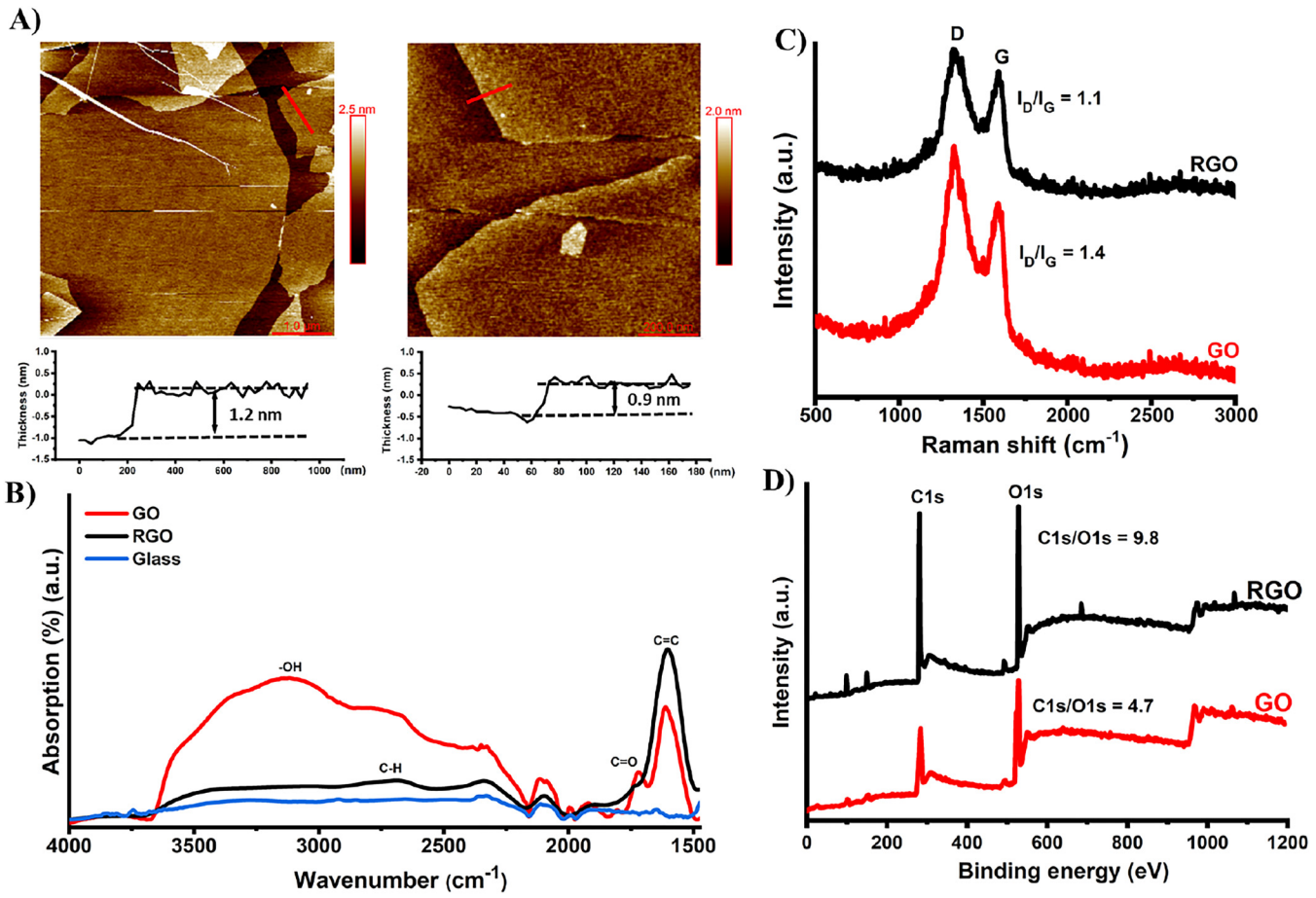

FIG. 2. Physiochemical characterization of GO and RGO. (a) AFM images depicting the surface morphology of GO and RGO flakes accompanied by the height profile. (b) FTIR spectra of neat clean glass, GO-, and RGO-coated glass substrate, displaying characteristic peaks for oxygen-containing groups in GO and their subsequent reduction in RGO. (c) The Raman spectra of GO and RGO revealing the D and G bands, with the I_D/I_G ratio decreasing for RGO. (d) XPS spectra for GO and RGO illustrating the C1s and O1s peaks and the area under the curve of carbon and oxygen 1s signals were taken along with the RSF for calculating C:O ratio.

1620 cm^{-1}, respectively [Fig. 4(b)].[31] In contrast, the FTIR spectrum of RGO showed significant reduction in hydroxyl and oxygen-containing carbonyl (–C = O) groups and retention of high alkenes (–C = C–) functional group peaks at ~1620 cm^{-1} reflecting the removal of oxygen functionalities and restoration of the sp^2 hybridization upon thermal reduction. However, some residual fraction of oxygen-containing groups often remains, as is evident from small shoulder and humps seen for carboxyl groups at 1720 cm^{-1}, making RGO distinct from pristine graphene.[32]

Figure 2(c) shows Raman spectra of GO- and RGO-coated substrates. Spot Raman spectra taken from GO- and RGO-coated substrates showed their characteristic D and G bands at 1325 and 1588 cm^{-1}. Furthermore, to understand the effect of thermal reduction on the removal of oxygenated functional groups from basal graphene surface and edges, we measured the I_D/I_G ratio as an indicator of defect density created by the presence of oxygenated functional groups on graphene sheets. I_D/I_G ratio of GO decreased from 1.4 to 1.1 for RGO after thermal reduction, indicating a partial restoration of sp^2 hybridization of a carbon network in graphene due to the removal of oxygenated functional groups. Figure 2(d) shows the XPS spectra of GO- and RGO-coated substrates with elemental carbon (C1s) and oxygen (O1s) peaks at 283 and 531 eV, respectively.[33] After thermal treatment of GO, the relative elemental ratio of C1s/O1s increased from 4.7 (for GO) to 9.8 (for RGO), indicating around 52% removal of oxygenated functional groups aligning with FTIR and Raman spectra suggesting a partial restoration of the graphene sp^2 carbon network.

B. Surface charge and surface potential measurement of GO- and RGO-coated substrates

For zeta potential measurements, the coated GO and RGO sheets were carefully scraped off the coated substrate and dispersed into an appropriate solvent to form a stable dispersed solution. The

average zeta potential of obtained GO solution was −37.5 mV, which can be attributed to the presence of negatively charged oxygenated functional groups on the graphene surface. After thermal reduction, the zeta potential decreased to −17 mV but still remained negative as shown in Fig. 3(a), indicating that during thermal treatment major fraction of negatively charged oxygenated functional groups were removed while some oxygenated functional groups were retained as evidenced by FTIR spectra.

Achieving a reliable evaluation of surface potential requires a thin coating over the underlying substrate to maintain contrast between the coated material and the substrate. However, the obtained full coverage coating of GO and RGO flakes may obscure the substrate completely, resulting in an equipotential surface across the scanned area hindering the accurate surface potential mapping. To address this challenge, we used a low concentration GO solution (0.1 mg/ml) to achieve a thin and less coverage coating on the silica substrate via spin coating followed by thermal treatment. This approach ensures that the underlying silica substrate remains partially visible, allowing us to maintain clear contrast during surface potential scans. The surface potential profile of indivisible GO and RGO sheets along with their height profile was evaluated using KPFM technology. The topographic image of GO and RGO with respective height profile is shown in Fig. 3(b), whereas Fig. 3(c) shows simultaneously obtained surface potential image of GO and RGO sheets. The height profile of GO and RGO showed thickness of 1.3 and 0.9 nm consistent with previous AFM thickness measurements. Surface potential imaging exhibited clear distinguished potential mapped areas (blue for GO, magenta for RGO) with respect to underneath silica substrate (yellow color). Measured surface potential of GO and RGO with respect to the silica substrate was 120 and 60 mV, respectively, as shown in Fig. 3(d). The high surface potential for GO can be attributed to the presence of high amount of ionizable oxygenated functional groups like hydroxyl and carboxyl groups, which creates localized charges and dipoles contributing to a high electrostatic potential on the GO surface. The decrease in surface potential upon thermal reduction for RGO indicated that most of oxygenated functional were removed leading to a decrease in surface charge density and promote restoration of the graphitic network increasing its conductivity in consistent with literature.[34,35] These change in surface potential for GO and RGO indicate they may have altered electronic interactions with adsorbed species.

Surface wettability of GBMs have shown to be regulated by multiple factors, including the underlying substrate, surface contamination, ambient environmental conditions, sample condition (freshly exfoliated versus non-freshly exfoliated), thickness (number of layers), intrinsic surface chemistry, surface roughness, and the specific measurement method employed.[36] Similar to these parameters, the surface potential of different GBMs can alter the distribution of charges and provide dipole moments on the surface, which can influence the ionic interaction between the GBM surface and water molecules, affecting wettability.[37] Thus, using one of the most classical techniques of the sessile water droplet method, we measured contact angle of the GO- and RGO-coated substrates. The GO-coated substrate with polar oxygenated functional groups and high surface potential showed low water contact angle of 38.2° resulting in wetting the surface. On other hand, RGO with low polar oxygenated functional groups and low surface potential resulted in high water contact angle of 89.8° on the surface [Fig. 3(e)]. The measured contact angles of GO (38.2°) and RGO (89.8°) are in close agreement with reported values, wherein GO typically exhibits hydrophilic behavior (30°–50°) and RGO displays increased hydrophobicity (80°–90°).[37,38] This consistency confirms the successful surface modification from GO to RGO and further supports the notion that changes in surface potential critically influence the wettability of graphene-based materials. Studies have

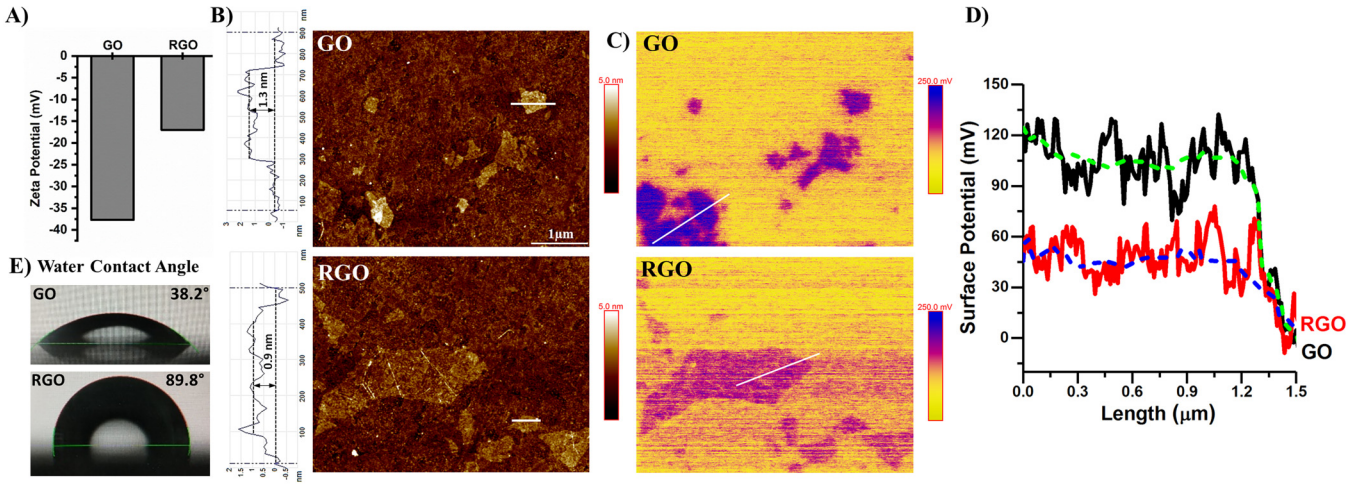

FIG. 3. Characterization of the surface properties of GO and RGO. (a) Zeta potential analysis of dispersed GO and RGO flakes. (b) Surface potential profiles of GO and RGO obtained through KPFM, accompanied by their respective height profiles. (c) GO and RGO surface potential map images captured concurrently with KPFM. (d) Surface potential measurements of GO and RGO with respect to the silica substrate. (e) Water contact angle micrographs of GO and RGO as a function of hydrophilicity.

shown that materials with high surface potential shows strong polar and electrostatic interactions with water molecules making them hydrophilic in nature, whereas surfaces with low surface potential reduces ionic interaction capacity with water resulting in high water contact angle on the surface making them hydroponic in nature.[39]

C. Fibronectin protein adsorption and interaction on GO- and RGO-coated substrates

The wettability of GO and RGO influenced by surface potential may further play a pivotal role in determining the initial interaction of GBMs with their biological microenvironment. To further elucidate the role of GO and RGO surface potential in modulating these interactions, we conducted a protein adsorption study using fibronectin, a most common protein found in the extracellular matrix (ECM). Figure 4(a) illustrates a quartz crystal microbalance plot showing progressive decrease in frequency over time, corresponding to the adsorption of FN onto GO and RGO substrates. A more rapid frequency shift was observed on RGO substrates compared to GO, with the frequency reaching saturation at −183 Hz for RGO and −80 Hz for GO. These frequency shifts correspond to average mass densities of 1079.7 ± 97.3 ng/cm^2 for RGO and 472 ± 68.1 ng/cm^2 for GO, which indicates that the RGO substrate exhibited approximately threefold greater adsorption of fibronectin compared to the GO substrate. Obtained QCM-D FN adsorption study was consistent with the results from fluorescence microscopy studies, which also revealed significantly higher adsorption of fluorophore-labelled FN on RGO surfaces compared to GO surfaces as shown in Fig. 4(b).

The high adsorption of FN on the RGO surface can be attributed to its low surface potential, hydrophobic nature, and reduced negative surface charge. These properties create an energetically favorable environment for the displacement of weakly interacting water molecules by FN adsorption. In addition, FN has an isoelectric point at *p*H 5.92, so it carries a net negative charge under physiological conditions. As a result, lower negative charge density on RGO surfaces reduces electrostatic repulsion, thereby promoting high FN protein adsorption. Consistent with our result, Lin *et al.* demonstrated that FN proteins exhibit less polarization when adsorbed onto negatively charged surfaces with low surface potential compared to those with high surface potential.[39] The reduced polarization of FN was attributed to the weaker electric field generated by surfaces with lower potential, which minimizes the distortion of the protein's charge distribution, leading to less electrostatic repulsion by negatively charged surfaces with low surface potential. Overall, these results indicated that the combination of hydrophobic interactions and reduced electrostatic repulsion due to low surface potential facilitates enhanced FN adsorption on RGO

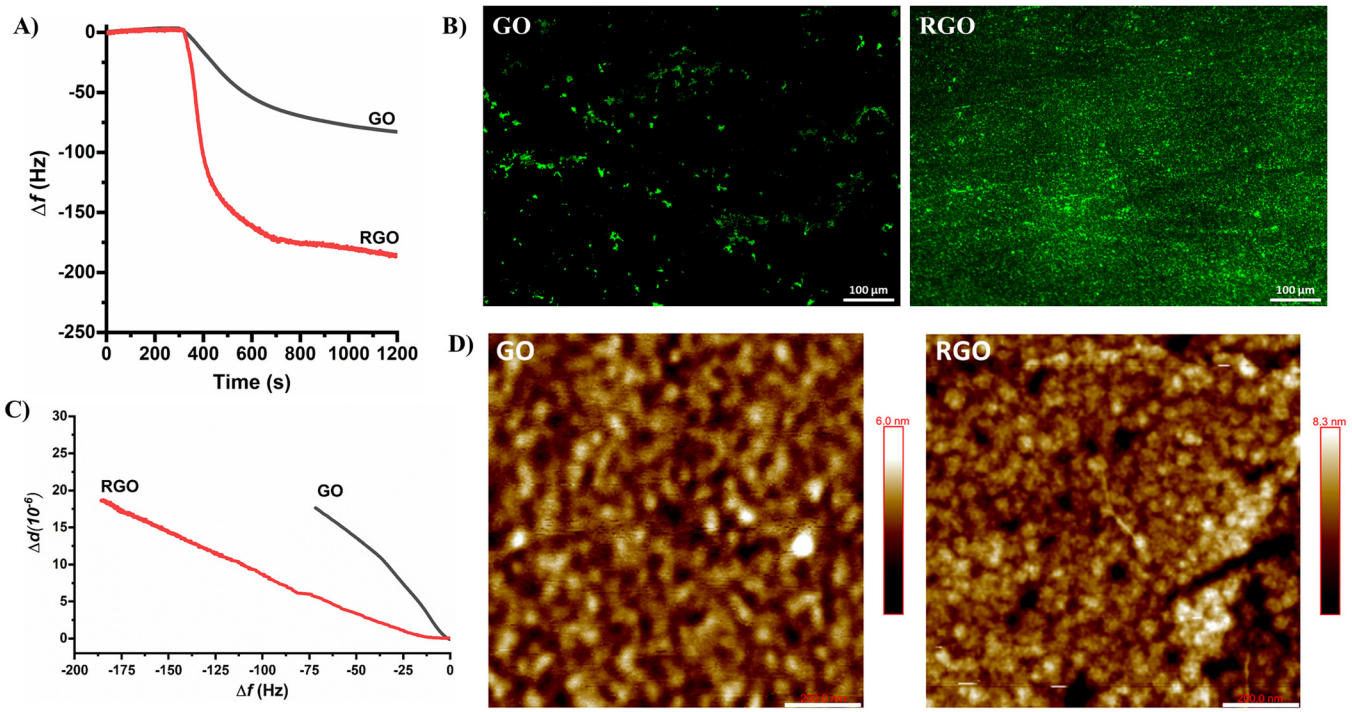

FIG. 4. Fibronectin adsorption on GO and RGO. (a) Real-time QCM-D adsorption profile of FN on GO and RGO. (b) Fluorescence microscopy images of adsorbed FN on GO and RGO (scale bar = 100 μm). (c) QCM dissipation per frequency ($\Delta D/\Delta F$) plot of FN on GO and RGO. (d) AFM images revealing structural morphology of FN on GO and RGO surfaces (scale bar = 200 nm).

compared to more negatively charged and high surface potential surfaces like GO.

Most of the study mainly concentrates on the macroscopic adsorption behavior of proteins on material surfaces and provides insights into the affinity and amount of protein adsorption on the material surface.[40,41] However, it is equally critical to evaluate the strength, nature of the interactions, molecular conformation, and stability between the adsorbed proteins and the materials surface as these factors directly influence the materials' biological performance. To gain a comprehensive understanding of protein-material interactions on GO and RGO having different surface potential, we studied the adsorption energy of FN on the GO- and RGO-coated surface by quantifying the dissipation per frequency (ΔD/ΔF) using QCM-D data, which provides insights into the hydrodynamic size, packing density, molecular conformation, and binding strength of surface-adsorbed proteins.[42] Studies have shown that a larger (ΔD/ΔF) ratio indicates loosely packed protein layers on the material surface, while changes in the slope of the (ΔD/ΔF) plot during protein adsorption reflect molecular rearrangements, highlighting dynamic conformational adaptations as the proteins stabilize their structure on the surface.[43,44] Figure 4(c) shows a plot of dissipation changes per frequency changes (ΔD/ΔF) for FN adsorption on GO- and RGO-coated surfaces.

FN on GO surfaces showed higher (ΔD/ΔF) value with a change in a slope value in comparison to the RGO surface [Fig. 4(c)], which suggests that FN molecules on the GO surface adsorb at a slower rate and form a more loosely elongated packed structure, indicating they might have undergone a conformational change during adsorption. On the other hand, adsorbed FN displays a single slope with lower (ΔD/ΔF) indicating a faster adsorption rate of FN and formation of a more rigid and compact structure. Tagaya *et al.* have very well highlighted that a higher slope in the dissipation versus frequency shift (ΔD/Δ*f*) plot during protein adsorption typically reflects lower adsorption rates and is often associated with unfolding of the protein upon surface interaction and undergoes conformational changes.[43] AFM study further confirmed the morphology and conformational changes of FN on the GO and RGO surfaces at nanoscale [Fig. 4(d)]. FN on GO showed elongated fibrillar structures, whereas FN on RGO appeared as globular compact structures. Several studies have pointed out that electrostatic interaction of FN on the material's surface regulates its native compact folded structure. FN on a surface with low negative charge density has shown minimal reorientation of the FN domain, as a result molecules adsorb immediately on the surface making a rigid compact structure as shown by a decreased dissipation factor on the RGO surface. On material with high negative charge density, FN has shown to mediate the slow rate of adsorption with unfolding of the compact structure into elongated structures due to rearrangement of the molecular structure in FN so that its polar or positive charged domains interact strongly with high negative charge surface. On a similar note, Renner *et al.* observed that fibronectin (FN) formed a rigid, compact, and densely packed layer on hydrophobic surfaces with a high carbon-to-oxygen ratio, such as poly (octadecene-alt-maleic anhydride) (POMA). In contrast, on hydrophilic surfaces with a low carbon-to-oxygen ratio, like poly (propene-alt-maleic anhydride) (PPMA), FN adopted a more flexible and elongated conformation, as evidenced by an increased ΔD/ΔF ratio.[44] These results suggested that the difference in carbon-to-oxygen ratios of GO and RGO surfaces influenced their surface potential, which might have played a significant role in modulating fibronectin (FN) electrostatic interactions at the molecular scale, thereby regulating its conformation upon adsorption.

D. Computational modelling of FN interaction with GO and RGO surface

To further investigate how graphene-based materials (GBMs) with varying carbon-to-oxygen (C/O) ratios having different surface potentials influence protein conformation through molecular interactions, we employed a computational simulation study. This approach allowed us to explore the molecular-scale mechanisms driving protein adsorption and conformational changes on GO and RGO surfaces, providing deeper insights into the role of surface properties in regulating protein-material interactions. The docking analysis demonstrated varying binding affinities and conformational stability of FN on GO and RGO, as illustrated in Figs. 5(a) and 5(b), respectively, highlighting the significance of surface potential in influencing protein-material interactions, aligning with the findings from fluorescence microscopy and AFM analyses.

For the molecular docking studies, we employed the minimized crystal structure of fibronectin and energy-optimized models of GO and RGO surfaces as the input conformations. Each docking simulation sampled roughly 50 conformations, with energy values for these conformers varying from approximately −0.5 to −3.9 kcal/mol, depending on the interaction surface. The conformer with the lowest energy was utilized to determine the docking scores (*C*-score), with the *C*-scores for FN adsorption onto GO and RGO recorded at −2.24 and −3.87, respectively [Fig. 5(c)], suggesting a greater binding affinity of FN to RGO in comparison to GO. The disparity in binding energy is attributed to the decreased surface potential of RGO, which enhances hydrophobic interactions and reduces electrostatic repulsion, thus fostering stable protein adsorption. The reduced surface potential of RGO, resulting from the elimination of oxygenated functional groups during thermal reduction, establishes a thermodynamically advantageous setting for FN attachment. The higher surface potential of GO likely induces electrostatic repulsion between the negatively charged FN molecules and the material surface, thereby lowering binding strength. Figure 5(d) illustrates the hydrophobicity and hydrogen bonding interaction maps of FN with GO and RGO, emphasizing the distinct binding mechanisms. FN-GO interactions were predominantly influenced by hydrogen bonding resulting from oxygenated functional groups, while FN-RGO demonstrated more robust hydrophobic interactions, which enhanced adsorption stability.

The analysis of RMSD confirmed the stability of the docked complexes. The RMSD values were 0.42 Å for FN-GO and 0.01 Å for FN-RGO, indicating a markedly more stable conformation of FN on RGO. The minimal deviation observed for FN on RGO indicates a rigid and well-anchored protein structure. In contrast, the higher RMSD for FN on GO suggests greater conformational flexibility, likely resulting from weaker interactions and increased molecular rearrangement across the surface. This is in line with experimental results from QCM-D and AFM, which showed that FN adopted an elongated and loosely packed conformation on GO while forming a compact rigid layer on RGO.

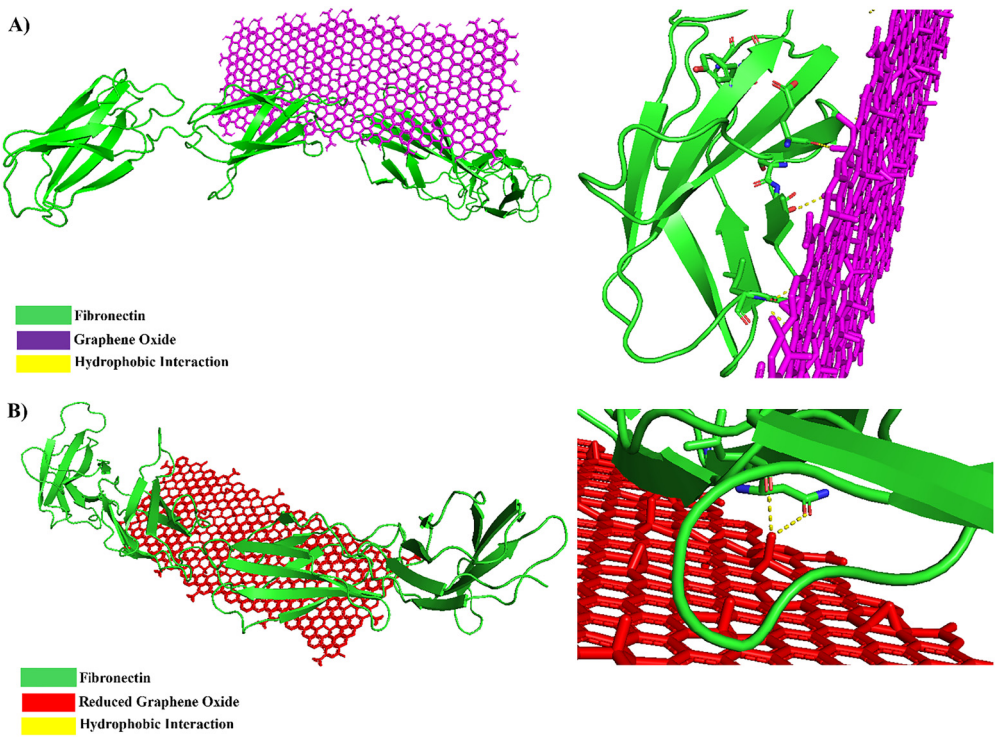

C)

Sample	C-Score	RMSD (Å)
Fibronectin- Graphene Oxide	-2.24	0.42
Fibronectin- Reduced Graphene Oxide	-3.87	0.01

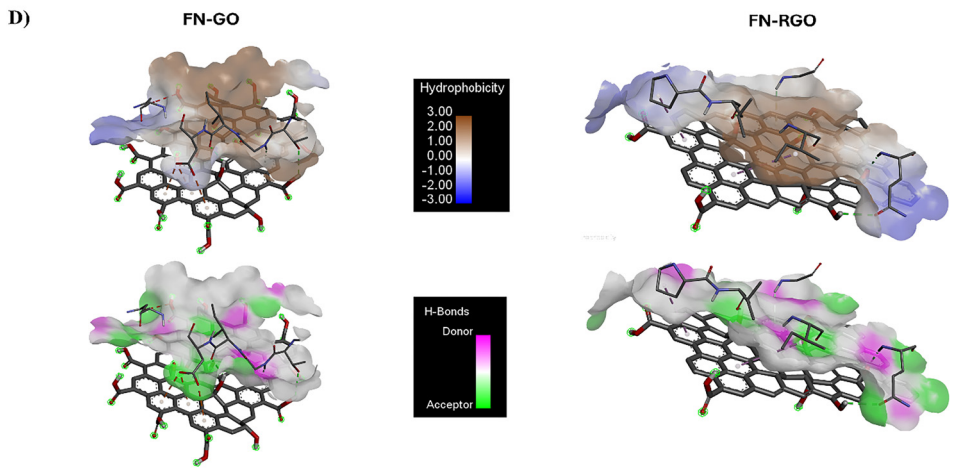

FIG. 5. Computational prediction of FN binding with GO and RGO. (a) Molecular docking of FN with GO highlighting hydrophobic interactions. (b) Molecular docking of FN with RGO highlighting hydrophobic interactions. (c) Affinity and stability analyses of FN with GO and RGO in terms of C-score and RMSD values. (d) Hydrophobicity and hydrogen bonding maps of FN interaction with GO and RGO.

Hydrophobic interactions significantly influenced FN adsorption onto RGO, supporting the hypothesis that reduced surface potential improves protein-material interactions by decreasing electrostatic repulsion. In contrast, the elevated surface potential of GO enhanced electrostatic interactions, resulting in increased protein rearrangements and reduced overall adsorption stability. The findings underscore the significant influence of surface potential on protein adsorption affinity, stability, and conformation at the molecular level. The improved FN binding to RGO highlights the importance of tweaking surface charge and chemistry in the development of graphene-based biomaterials with regulated biointerface characteristics.

IV. LIMITATIONS OF THE STUDY

One of the main goals of this study was to evaluate how the surface potential of GBMs influences protein adsorption and molecular interaction. However, in GBMs, it is really challenging to isolate chemistry and surface potential, which are inherently interlinked in graphene-based materials, making it one of the limiting and challenging factors. This work sets the platform to initiate thinking around the role of the surface potential of GBMs in regulating protein interactions, emphasizing the need to extend this exploration further.

In relation to surface potential, in this study, only two levels of surface potential variation (+120 mV for GO and +60 mV for RGO) were considered; however, for a better in-depth understanding, one should think of a broader range of surface potentials, which provide deeper insights and strengthen the parallels with studies on surface chemistry modifications. Such investigations, however, demand precise control, reduction of experimental variability, and rigorous optimization to precise control of surface potential variation with minimal variation in chemistry of GBM, through several parameter optimization, which can be very challenging and may be considered in future studies.

Another limitation of this work is that it mainly focuses on a single-protein system, specifically fibronectin [as a simple foundational model keeping standardized conditions like *p*H (7.4) and isotonic PBS buffer to mimic a biomimetic environment to provide insights into the influence of surface potential on adsorption behavior], which does not fully capture the complexity, dynamics, and competitive adsorption of multicomponent protein environments encountered in physiological conditions governed by phenomena like the Vroman effect. This multicomponent competitive adsorption behavior is influenced by factors such as different protein concentration, size, charge, diffusion kinetics, *p*H, and binding energy, which can significantly alter the nature and conformation of the final protein layer on materials with different surface potentials.[45,46]

V. CONCLUSIONS

This study focuses on the impact of surface potential on protein interactions with GO and RGO substrates. Spin-coated GO substrate was thermally reduced to RGO to obtain two distinct GBM having distinct surface potential. GO having rich amount of oxygenated functional groups showed high surface potential (+120 mV) in comparison to RGO (+60 mV) with reduced oxygenated functional groups. Reduction in surface potential on the RGO surface supported enhanced FN adsorption with strong interaction forming globular structure on its surface, whereas FN on GO showed low adsorption with elongated fibrillar structures with an apparent formation of a protein network. These results suggested that the obtained GO and RGO having difference in carbon-to-oxygen ratios can influence their surface potential, which might have played a significant role in modulating fibronectin (FN) electrostatic interactions at the molecular scale, thereby regulating its molecular conformation upon adsorption. Additionally, the molecular docking simulation supported these experimental results, showing that FN-RGO interactions were stronger than FN-GO interactions, as indicated by a lower C-score and a lower RMSD. The reduced surface potential of RGO lowered electrostatic repulsion and strengthened hydrophobic interactions, resulting in a more stable binding conformation. Overall, the study highlights the importance of surface potential in protein adsorption, binding stability, and molecular conformation on GBMs, providing insights into the development of graphene-based biomaterials with improved biointerface properties for tissue engineering and biomedical applications.

SUPPLEMENTARY MATERIAL

See the supplementary material for the following: Figure S1: Digital images of RGO-coated glass substrate, GO-coated glass substrate, and neat glass substrate; Fig. S2: FTIR spectra of neat clean glass, GO-coated glass, and RGO-coated glass substrate.

ACKNOWLEDGMENTS

The authors would like to thank Prof. Nikolina Šoštarić of Department of Bionanoscience, TUD for her inputs in computational studies and proofreading. Figures were created using BioRender.com. The authors thank Prof. Sapun Parekh for providing GO and helping with its characterization using MPIP facility, Germany. The authors acknowledge funding support received from MFIRP, IITD-TUD (No. MI02979G).

AUTHOR DECLARATIONS

Conflict of Interest

The authors have no conflicts to disclose.

Ethics Approval

No experiments on animal or human subjects were used for the preparation of the submitted manuscript. Ethics approval is not required.

Author Contributions

Rohit: Conceptualization (lead); Data curation (lead); Formal analysis (equal); Investigation (equal); Methodology (equal); Writing – original draft (lead); Writing – review & editing (equal). **Rachayita Bharadwaj:** Conceptualization (equal); Data curation (equal); Formal analysis (equal); Methodology (equal); Writing – original draft (equal). **Chandrashish Roy:** Formal analysis (supporting); Methodology (supporting); Validation (equal).

Sourabh Ghosh: Formal analysis (supporting); Supervision (supporting); Writing – review & editing (supporting). **Sachin Kumar:** Conceptualization (lead); Data curation (lead); Formal analysis (equal); Funding acquisition (lead); Methodology (supporting); Supervision (lead); Writing – original draft (supporting); Writing – review & editing (lead).

DATA AVAILABILITY

The data that support the findings of this study are available from the corresponding author upon reasonable request.

REFERENCES

[1]T. R. Kyriakides, in *Host Response to Biomaterials* (Academic, 2015), pp. 81–116.
[2]P. Roach, D. Farrar, and C. C. Perry, J. Am. Chem. Soc. **127**, 8168 (2005).
[3]T. A. Horbett, J. Biomed. Mater. Res., Part A **106**, 2777 (2018).
[4]R. Kumar, D. P. Singh, R. Muñoz, M. Amami, R. K. Singh, S. Singh, and V. Kumar, Mater. Today Chem. **33**, 101750 (2023).
[5]W. Xue, J. Du, Q. Li, Y. Wang, Y. Lu, J. Fan, S. Yu, and Y. Yang, Tissue Eng. Part B: Rev. **28**, 1121 (2022).
[6]F. Batool, S. Muhammad, R. Muazzam, M. Waqas, Z. Ullah, S. Roy, K. Wang, and B. Guo, Smart Mater. Med. **6**, 120 (2025).
[7]J. Li, H. Zeng, Z. Zeng, Y. Zeng, and T. Xie, ACS Biomater. Sci. Eng. **7**, 5363 (2021).
[8]S. Kumar and S. H. Parekh, Commun. Chem. **3**, 1 (2020).
[9]S. Ghosh and K. Chatterjee, Int. J. Nanomed. **15**, 5991 (2020).
[10]W. C. Lee, C. H. Y. X. Lim, H. Shi, L. A. L. Tang, Y. Wang, C. T. Lim, and K. P. Loh, ACS Nano **5**, 7334 (2011).
[11]S. Kumar and S. H. Parekh, ACS Appl. Mater. Interfaces **13**, 2 (2021).
[12]K. Ohta, H. Monma, and S. Takahashi, J. Biomed. Mater. Res. **55**, 409 (2001).
[13]K. Wang, C. Zhou, Y. Hong, and X. Zhang, IF **2**, 259 (2012).
[14]X. D. Zhu, H. S. Fan, C. Y. Zhao, J. Lu, T. Ikoma, J. Tanaka, and X. D. Zhang, J. Mater. Sci.: Mater. Med. **18**, 2243 (2007).
[15]V. Panchal, R. Pearce, R. Yakimova, A. Tzalenchuk, and O. Kazakova, Sci. Rep. **3**, 2597 (2013).
[16]R. Pearce, T. Iakimov, M. Andersson, L. Hultman, A. Lloyd Spetz, and R. Yakimova, in *Proceedings of SENSORS*, Waikoloa, HI, 2010 (IEEE, 2010), pp. 898–902.
[17]G. L. Hao, X. Qi, J. Li, L. W. Yang, J. J. Yin, F. Lu, and J. X. Zhong, Solid State Commun. **151**, 818 (2011).
[18]P. Kuang and K. Constant, in *Wetting and Wettability* (IntechOpen, 2015), Chap. 4, p. 85.
[19]A. Kovtun, D. Jones, S. Dell'Elce, E. Treossi, A. Liscio, and V. Palermo, Carbon **143**, 268 (2019).
[20]N. M. Das, A. K. Singh, D. Ghosh, and D. Bandyopadhyay, Nanoscale Adv. **1**, 3727 (2019).
[21]A. Chlanda, E. Walejewska, K. Kowiorski, M. Heljak, W. Swieszkowski, and L. Lipińska, Micron **146**, 103072 (2021).
[22]D. J. Leahy, I. Aukhil, and H. P. Erickson, Cell **84**, 155 (1996).
[23]E. F. Pettersen, T. D. Goddard, C. C. Huang, G. S. Couch, D. M. Greenblatt, E. C. Meng, and T. E. Ferrin, J. Comput. Chem. **25**, 1605 (2004).
[24]M. F. Sanner, A. J. Olson, and J. Spehner, Biopolymers **38**, 305 (1996).
[25]O. Trott and A. J. Olson, J. Comput. Chem. **31**, 455 (2010).
[26]C.-H. Chuang *et al.*, Sci. Rep. **4**, 1 (2014).
[27]A. L. Liboon, Jr., S. R. Cabo, and R. Candidato, Jr., Biointerface Res. Appl. Chem. **13**, 245 (2022).
[28]E. György, A. Pérez del Pino, J. Roqueta, C. Sánchez, and A. G. Oliva, Colloids Surf., B **104**, 169 (2013).
[29]B. S. Yilbas, A. Ibrahim, H. Ali, M. Khaled, and T. Laoui, Appl. Surf. Sci. **442**, 213 (2018).
[30]C. L. Leverette, C. Wills, M. A. Perkins, and S. A. Jacobs, J. Chem. Educ. **86**, 719 (2009).
[31]F.-P. Du, N.-N. Cao, Y.-F. Zhang, P. Fu, Y.-G. Wu, Z.-D. Lin, R. Shi, A. Amini, and C. Cheng, Sci. Rep. **8**, 1 (2018).
[32]F. T. Johra and W.-G. Jung, Appl. Surf. Sci. **357**, 1911 (2015).
[33]J. H. Chu *et al.*, Nat. Commun. **5**, 3383 (2014).
[34]P. Das, S. Ibrahim, K. Chakraborty, S. Ghosh, and T. Pal, Sci. Rep. **14**, 294 (2024).
[35]D. Öztekin, H. Arbağ, and S. Yaşyerli, "Preparation of RGO with enhanced electrical conductivity: Effects of sequential reductions of L-ascorbic acid and thermal," Arab. J. Sci. Eng. (published online 2025).
[36]S. R. Carlson, O. Schullian, M. R. Becker, and R. R. Netz, J. Phys. Chem. Lett. **15**, 6325 (2024).
[37]J. Rafiee, X. Mi, H. Gullapalli, A. V. Thomas, F. Yavari, Y. Shi, P. M. Ajayan, and N. A. Koratkar, Nat. Mater. **11**, 217 (2012).
[38]G. Eda and M. Chhowalla, Adv. Mater. **22**, 2392 (2010).
[39]J.-H. Lin *et al.*, Langmuir **30**, 10328 (2014).
[40]F. Romero-Gavilán *et al.*, J. Biol. Inorg. Chem. **26**, 715 (2021).
[41]E. Steinrücken, L. Diehl, T. Wissel, G. Buntkowsky, H. S. Varol, A. Andrieu-Brunsen, and M. Vogel, J. Chem. Phys. **162**, 084702 (2025).
[42]J. A. Jackman, A. Rahim Ferhan, and N.-J. Cho, Chem. Soc. Rev. **46**, 3615 (2017).
[43]M. Tagaya, Polym. J. **47**, 599 (2015).
[44]L. Renner, T. Pompe, K. Salchert, and C. Werner, Langmuir **21**, 4571 (2005).
[45]H. S. Varol, D. Kaya, E. Contini, C. Gualandi, and D. Genovese, Mater. Adv. **5**, 8351 (2024).
[46]X. Chen, J. Chen, and N. Huang, Biosurf. Biotribol. **8**, 1 (2022).